Motion Control Design for an Economical Robotic Walking Support System: The Robotic Cane

Yong-Zeng Zhang and Syh-Shiuh Yeh

Abstract—This study aims at the development of a motion control design for controlling robotic walking support systems using a force-controlled motion command generator so that robotic walking support systems can provide smooth motions to users with desired motion speeds. The motion control laws are implemented with a low-pass filter that has adjustable gain and bandwidth. Through the cooperation of motion control laws and force-sensing results, the force-controlled motion command generator can generate smooth motion commands to smoothly drive robotic walking support systems. A simple and low-cost biaxial force-sensing device is developed in this study to estimate the equivalent interactive forces between the user and the robotic walking support system. A calibration procedure is also developed to obtain the virtual spring coefficient and to design an estimation method that can be used with the biaxial force-sensing device. A robotic walking support system, the robotic cane, is developed with two operation modes, autonomous motion mode (AMM) and manual motion mode (MMM), for testing the proposed motion control approach, and several tests and experimental results are presented to show the validity of the proposed approach.

Index Terms—robotic walking support system, motion control design, force-controlled motion command generator, force-sensing device, robotic cane

I. INTRODUCTION

IN a society that is constantly aging, walking support systems have become important for the elderly because they can assist them in their daily activities so that they can regain independence and have improved quality of life. The most common walking support systems include crutches, walkers, and canes. A crutch is usually used as a tool for patients suffering from lower limb problems when they walk large distances. Therefore, aged people whose lower limbs are in normal condition but face difficulties in walking may use walkers or canes to help them walk. Such devices are usually used to maintain body balance, support weight, train to walk, and increase muscle strength of lower limbs. Besides,

Yong-Zeng Zhang is with the Institute of Mechatronic Engineering, National Taipei University of Technology, Taipei, Taiwan (e-mail: yzzhang@ntut.edu.tw).

Syh-Shiuh Yeh is with the Department of Mechanical Engineering, National Taipei University of Technology, Taipei, Taiwan (phone: +886-2-2771-2171; fax: +886-2-2731-7191; e-mail: ssyeh@ntut.edu.tw).

canes are also available for visually impaired people to help them detect road situations while walking. Although conventional walking support systems are usually used to solve mobility problems in the elderly, they are considered as passive devices and their motions strictly depend on the user's decision to apply forces/torques to them. Therefore, the users of these conventional walking support systems must be capable of functions such as sufficient cognitive function, good vision, judgment, and endurance, all of which are difficult to satisfy for the elderly because these functions degrade with aging.

In recent decades, because of the rapid development of robotic technologies, including actuating and sensing devices, robotic technologies are widely and diversely being introduced into conventional walking support systems, and the developed robotic walking support systems can normally provide much better walk-assisting performances. Lacey and Dawson-Howe [1] described an application of mobile robot technology to provide robot mobility aid for the frail blind; further, the PAM-AID mobile robot [2] consisting of a walking frame with wheels was developed to help avoid obstacles and physically support the person walking. For helping the elderly live independently in their private living environments, a robotic assistant named Care-O-bot II [3] was developed with adjustable walking supporters to support and guide the elderly people safely while they walked in indoor environments. Hirata et al. [4] proposed a passive intelligent walker named RT Walker to assist elderly and handicapped people walking in both indoor and outdoor environments. The developed adaptive motion control algorithm facilitates the mechanical behaviors of the RT Walker to adapt to user operation, and it helps avoid obstacles according to the extracted environmental information. Chuy Jr. et al. [5][6] developed the Walking Helper, which considers user operation characteristics to aid users in controlling their walking support system; further, Chuy Jr. et al. [7] developed a motorized robotic walking support system based on the passive behavior concept proposed by Hirata et al. [4] to enhance the interaction between the walking support system and the user. Wasson et al. [8] presented an operation system that can infer the navigational intent of a walker's user based on the measured forces and moments applied to the handles of the walker. Morris et al. [9] proposed a robotic walker that integrates a haptic interface and a robot localization and navigation system to provide mobility aid to frail elderly people with cognitive impairment. Sabatini et al. [10] developed a motorized rollator that is equipped with

force, ultrasonic, and infrared sensors to support elderly people in walking while avoiding collisions. Spenko et al. [11] developed a smart walker that provides support, guidance, and health monitoring for the elderly in an assisted living facility. The developed smart walker uses a six-axis force/torque sensor attached at the walker's handle as the main control input interface. Further, a shared adaptive control algorithm was developed to control the smart walker by a computer controller such that the smart walker gently guided the user. Although current successfully developed robotic walkers can offer support and safety guidance, their larger size hinders normal footsteps. Therefore, Spenko et al. [11] developed a smart cane that provides functions similar to those of the smart walker. Although some cane robots such as the Walking Guide Robot [12], RoJi Robot [13], Guide Cane Robot [14], and the Robotic Cane proposed by Aigner and McCarragher [15] can provide good guiding performances for the visually impaired and the elderly, they cannot physically support the elderly during walking.

Although existing researches have demonstrated important results, meeting the needs of the elderly, such as the requirement of smooth motion and low-cost force-sensing devices for controlling robotic walking support systems, remains a challenge. Despite high-level applications such as walking guidance and health monitoring being useful for the elderly during walking, motion control design of robotic walking support systems is important because the motion results of robotic walking support systems significantly affect the walking behaviors of the elderly. Some existing researches have focused on the study of the interaction behaviors between humans and an applied robotic walking support system by considering the dynamic characteristics of the applied robotic walking support system. However, the motion control system of robotic walking support systems must be implemented by considering the design of a motion command generator in order to provide smooth motion commands and to smoothly guide the elderly with the desired walking speeds.

In this study, the design of a force-controlled motion command generator is newly developed by considering the interactive forces/torques between humans and a robotic walking support system. The system can provide smooth motion with the desired speed of motion. In order to detect interactive forces/torques between humans and the robotic walking support system, a force/torque sensor is an essential component. However, sensors used to detect the interactive forces/torques in robotic walking support systems are usually designed for industrial applications, and they are normally expensive. Therefore, it is desired to design a cheap and simple force-sensing device that can be used to control robotic walking support systems and can thus reduce the cost for wide applications and general users. In this study, a simple biaxial force-sensing device is developed for estimating the interactive forces between humans and robotic walking support systems. In addition, methods of calibration and control using the force-sensing device are addressed.

In order to illustrate the design and application of the force-controlled motion command generator and the biaxial force-sensing device, a robotic walking support system, the robotic cane, is developed with adequate motion control design. The robotic cane is composed of a two-wheeled mobile platform with three range sensors, a cane-stick with handgrip, and a biaxial force-sensing device. Moreover, the robotic cane is designed to provide the following two operation modes:

- Autonomous motion mode (AMM): the robotic cane autonomously moves in walking environments along preplanned motion paths with the desired linear and angular velocities according to the signals sensed by range sensors.
- Manual motion mode (MMM): the robotic cane moves along preplanned motion paths with the adjustable linear velocity command closely related to the forces exerted by the user's hand.

Several simulations and experiments are carried out to test the execution performances of the force-controlled motion command generator implemented in the motion control design of the robotic cane. The experimental results indicate that the motion control design with the force-controlled motion command generator allows the robotic cane to execute different motions according to the selected operation modes.

This paper is organized in detail as follows. Section II presents the mechanical design of the robotic cane. The mechanism of the biaxial force-sensing device is also presented in this section. Section III to Section VI describe the motion control design of the robotic cane. Section III illustrates the architecture of motion control design; Section IV presents the design and selection of motion paths for the robotic cane; Section V presents the design of the force-controlled motion command generator; and Section VI describes the motion control laws cooperating with the force-controlled motion command generator. Section VII shows some simulation and experimental results of cases when the robotic cane executes different motions. Calibration and tests of the biaxial force-sensing device are also introduced in this section. Section VIII concludes this paper.

II. Mechanical Design of the Robotic Cane

Fig. 1 shows the design of the robotic cane. The robotic cane consists of three main parts: a cane-stick with handgrip, a force-sensing device, and a two-wheeled mobile platform. The two-wheeled mobile platform is equipped with two standard drive wheels, two castor wheels, main control unit, main power and auxiliary power units, ultrasonic range sensor, two infrared range sensors, and a touch-screen panel. The two standard drive wheels are used to drive the mobile platform by the differential spinning speeds of the left and right drive wheels such that the mobile platform can execute linear motion and rotational motion about the instantaneous center of rotation (ICR). The two castor wheels are free rotation wheels and are used to support the mobile platform. The motion control design is implemented in the main control unit composed of a data acquisition board, a motion control board, and a personal computer (PC) with a Pentium dual-core CPU. The main control unit receives sensing signals from force-sensing device and ultrasonic and infrared range sensors; the main control unit also sends the generated control signals to two standard drive wheels to control the motion of the mobile platform. The main power unit provides the required power to

the main control unit, the force-sensing device, the ultrasonic and infrared range sensors, and the touch-screen panel; the auxiliary power unit provides the required power to the two standard drive wheels. The ultrasonic range sensor is used to detect the distance from the front obstacles; the infrared range sensors are installed on the right and left sides at the front of the mobile platform to detect the distances of front-right and front-left obstacles. The touch-screen panel is used as the human-machine interface such that the users can set motion parameters such as the control gains of the motion control laws, the maximum and minimum motion speeds, and so on. Moreover, the touch-screen panel can be used to display the status of the robotic cane.

The design integrates a cane-stick with a mobile platform through a force-sensing device. The cane-stick is fixed to the force-sensing device, and it can slightly rotate about the center point of the device along the normal and lateral directions, as shown in Fig. 1. When using the robotic cane, the user's hand is placed on the handgrip and the robotic cane guides the user through the two-wheeled mobile platform. There are two operation modes of the robotic cane: AMM and MMM. By using the ultrasonic range sensor and the infrared range sensors, the robotic cane can estimate the distance from the mobile platform to the detected obstacles, and it can move autonomously according to the motion control design for avoiding obstacles. Therefore, the AMM can support and safely guide the user walking in living environments. For operation in the MMM, the user must hold the handgrip of the cane-stick. When the handgrip is moved along the positive normal direction by hand, the force-sensing device detects forces, and the mobile platform moves forward according to the motion control design developed in this study. This also applies to backward and lateral movements. However, for providing safety, the motion for obstacle avoidance is enabled when the robotic cane detects obstacles.
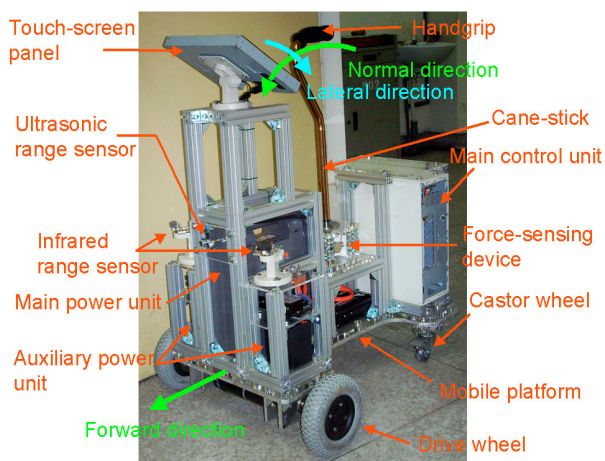

Fig. 1. The robotic cane.

Although there are many multi-axis force sensors available in the market, most of them are expensive and their multi-axis sensing capabilities are usually redundant for the purpose of controlling two-wheeled mobile platforms. Therefore, in this study, we have developed a simple biaxial force-sensing device as shown in Fig. 2. A universal joint is designed to carry two angular movement detection devices, and in this study, two potentiometers as the angular movement detection

devices are used to detect two rotating angles of the designed universal joint when relative angular movement between the upper and lower plates occurs. A connection stick with a sliding mechanism is designed to connect the upper plate and the universal joint such that the angular movements of the upper plate can be detected by potentiometers attached to the designed universal joint. The sliding mechanism on the connection stick makes the upper plate move along the radial direction of the universal joint without damaging the universal joint. Four spring devices are used to support the upper and lower plates. The cane-stick shown in Fig. 1 is connected with the upper plate through a supporter, and the force-sensing device connects to the mobile platform through the lower plate. The supporter provides fixed connection between the cane-stick and the upper plate of the force-sensing device, and the lower plate of the force-sensing device is fixed on the mobile platform, as shown in Fig. 1. Therefore, the cane-stick can slightly rotate about the center of the force-sensing device along the normal and lateral directions, as shown in Fig. 1.

Since the upper plate is connected to the cane-stick and the lower plate is connected to the mobile platform, relative angular movements between the upper and the lower plates occur when the user's hand exerts forces on the handgrip of the cane-stick. By applying Hooke's Law, we can estimate the equivalent forces exerted by the user's hand. Further, the estimated equivalent forces can be used later for the control of the mobile platform. In this study, since it is difficult to precisely estimate the applied forces, a method is developed to estimate the equivalent forces exerted by the user's hand.
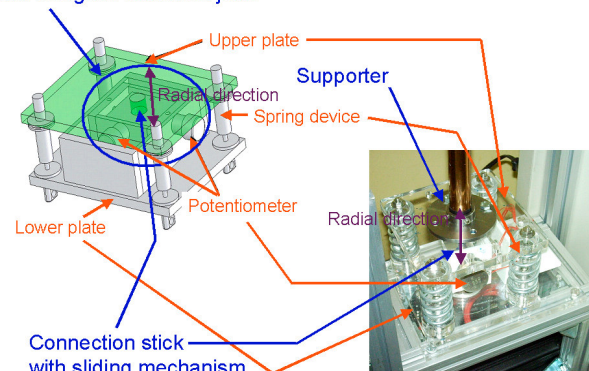

Fig. 2. The biaxial force-sensing device.

III. MOTION CONTROL DESIGN OF THE ROBOTIC CANE

In this study, as shown in Fig. 3, the motion control design of the robotic cane includes the design of the motion command generator and the design of motion control laws. By referring to the given motion paths that are preplanned by the user's operation and the status of range sensors, the motion command generator is designed to generate motion commands such as the linear and angular velocities for motion control laws. The motion control laws are developed to generate servo commands such as the spinning speeds of the left and right drive-wheels for the servomechanisms of the mobile platform. Therefore, three important designs are required, including motion path design, motion command generator design, and motion control law design. In this study, since the motion command generator is designed to generate motion commands by referring to the interactive forces

between the user and the robotic cane, it is also named the force-controlled motion command generator. Usually, an interpolation algorithm is required in the design of the motion command generator in order to interpolate the preplanned motion paths. The interpolation algorithm that considers the interactive forces is thus developed in this study. Moreover, the kinematics of the two-wheeled mobile platform is applied to the design of the motion control laws such that the robotic cane can execute different operation modes such as the AMM and the MMM for different walking assistance. These three designs are described in detail in the following sections.
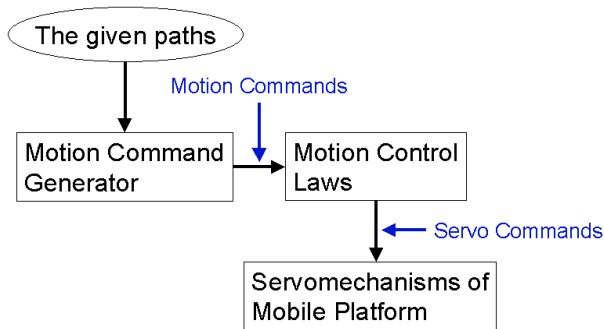
Fig. 3. Motion control architecture of the robotic cane.

IV. MOTION PATH DESIGN FOR ROBOTIC CANE

Fig. 4 shows the five preplanned motion paths when the robotic cane moves forward. In this study, the parametric curve is employed in the design of preplanned motion paths because of the following reasons:

- A unified mathematical model can be used to represent different motion paths. Therefore, only one mathematical model is used to represent five motion paths in this study.
- The shapes of motion paths can be modified easily by manipulating the shape-control parameters such as control points, weights, and knots. Therefore, the shapes of motion paths can be changed without changing the mathematical model.

In Fig. 4, "Path F" is a straightforward path. "Path FR1" and "Path FR2" are curve paths with large and small radii of curvature at the beginning, respectively. Thus, "Path FR1" and "Path FR2" can make the mobile platform move to the right with different motion speeds such that the robotic cane moves to the right slowly or quickly. Similarly, "Path FL1" and "Path FL2" are curve paths with different radii of curvature, and they can make the robotic cane moving to the left slowly or quickly. The selection of motion paths depends on the status of the range sensors and that of the force-sensing device. For operation in the AMM, the motion path "Path FL1" is selected in case the obstacles appear on the right side of the robotic cane. If the obstacles appear on both the front and right sides of the robotic cane, the motion path "Path FL2" is selected for quickly and urgently turning the robotic cane. Table I tabulates the selection of motion paths depending on the status of the front, left, and right range sensors. In Table I, the status of the range sensors is ON if the distance from the detected obstacles is smaller than a threshold value. The STOP path denoted in Table I represents the occurrence of undetermined conditions, for instance, when the obstacles surround the robotic cane and when the obstacles are located only in front of the robotic cane. For

such undetermined conditions, the motion of the robotic cane depends on the user's selection, and the operation of the robotic cane switches to the MMM. In this study, the motion path of the robotic cane is updated periodically in order to avoid obstacles in walking environments.
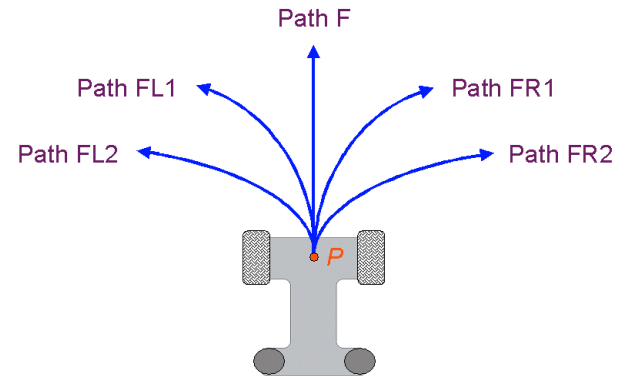

Fig. 4. The five preplanned motion paths of the robotic cane.

In order to select the motion path of the robotic cane during operation in the MMM, the operating range of the force-sensing device is divided into five sub-ranges, as shown in Fig. 5. Table II further tabulates the selection of motion paths depending on the sub-ranges R1, R2, R3, R4, and R5. For instance, the motion path "Path F" is selected in case the force-sensing device is operated in the sub-range "R3" by pushing the handgrip of the cane-stick along the positive normal direction. If the user pushes the handgrip of the cane-stick along the positive lateral direction, the force-sensing device is operated in the sub-range "R1," and the motion path "Path FL2" is selected for turning the robotic cane. In the operation in the MMM, the motion path of the robotic cane is also updated periodically. However, the operation of the robotic cane automatically switches to the AMM for choosing adequate motion paths in order to avoid collisions with obstacles.
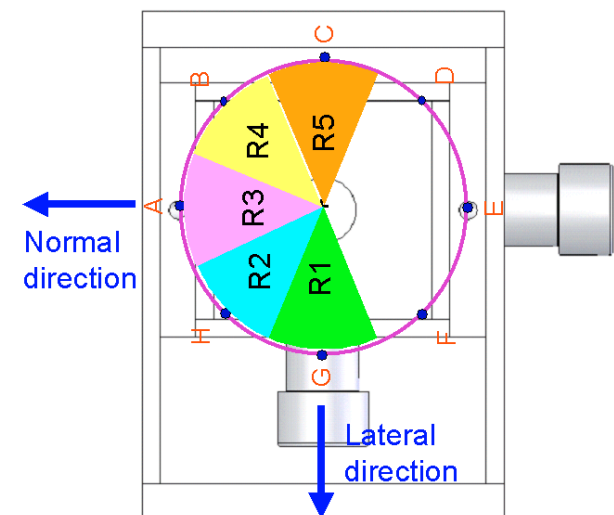

Fig. 5. The five sub-ranges for operating the force-sensing device.

TABLE I
THE SELECTION OF MOTION PATHS (AMM)

	Front ultrasonic range sensor is OFF		Front ultrasonic range sensor is ON	
	Right infrared range sensor is		Right infrared range sensor is	
	OFF	ON	OFF	ON
Left infrared range sensor is OFF	Path F	Path FL1	STOP	Path FL2
Left infrared range sensor is ON	Path FR1	Path F	Path FR2	STOP

TABLE II
THE SELECTION OF MOTION PATHS (MMM)

	Sub-range				
	R1	R2	R3	R4	R5
Motion Path	Path FL2	Path FL1	Path F	Path FR1	Path FR2

V. DESIGN OF THE FORCE-CONTROLLED MOTION COMMAND GENERATOR

Since the preplanned motion paths are represented by parameter curve functions, the motion command generator shown in Fig. 3 requires an interpolation algorithm to interpolate the given motion path and successively generate the interpolated points on the given motion path, as shown in Fig. 6. A parameter iteration method is thus developed to interpolate the parametric curve function, and the interpolated points are obtained by computing the curve function with the iterated parameters [16].
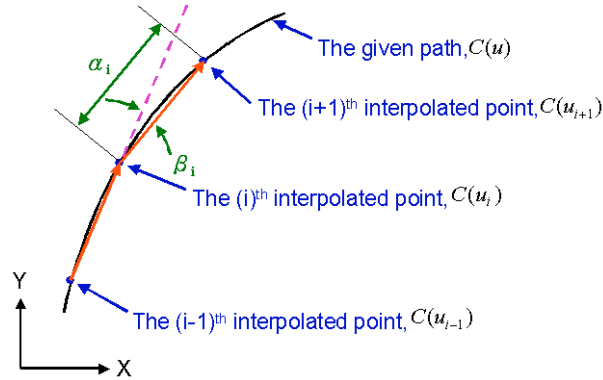

Fig. 6. The successive interpolated points on the given path.

Suppose that $C(u)$ is a parametric curve function that represents the given motion path, and the time function u is the curve parameter. The curve speed $V(u)$ and curve acceleration $A(u)$ can be derived as follows:

$$V(u) = \frac{dC(u)}{dt} = \frac{dC(u)}{du} \cdot \frac{du}{dt} \tag{1}$$

$$A(u) = \frac{d^2C(u)}{dt^2} = \frac{dC(u)}{du} \cdot \frac{d^2u}{dt^2} + \frac{d}{dt}\left(\frac{dC(u)}{du}\right) \cdot \frac{du}{dt}$$

$$= \frac{dC(u)}{du} \cdot \frac{d^2u}{dt^2} + \frac{d^2C(u)}{du^2} \cdot \left(\frac{du}{dt}\right)^2 \tag{2}$$

The functions D_i^u, D_i^t, D_i^{u2}, and D_i^{t2} are defined as follows:

$$D_i^u = \frac{dC(u)}{du}\bigg|_{u=u_i} \ ; \ D_i^t = \frac{dC(u)}{dt}\bigg|_{t=t_i} \tag{3}$$

$$D_i^{u2} = \frac{d^2C(u)}{du^2}\bigg|_{u=u_i} \ ; \ D_i^{t2} = \frac{d^2C(u)}{dt^2}\bigg|_{t=t_i} \tag{4}$$

where u_i denotes the value of u at time $t = t_i$. Then, (1) and (2) can be rewritten as follows:

$$V(u_i) = D_i^t = D_i^u \cdot \frac{du}{dt} \tag{5}$$

$$A(u_i) = D_i^{t2} = D_i^u \cdot \frac{d^2u}{dt^2} + D_i^{u2} \cdot \left(\frac{du}{dt}\right)^2 \tag{6}$$

Using (3) and (4), (5) and (6) can be further rewritten as follows:

$$\langle D_i^t, D_i^t \rangle = \langle D_i^u, D_i^u \rangle \cdot \left(\frac{du}{dt}\right)^2 \tag{7}$$

$$D_i^{t2} \cdot \langle D_i^u, D_i^u \rangle$$

$$= D_i^u \cdot \langle D_i^u, D_i^u \rangle \cdot \frac{d^2u}{dt^2} + D_i^{u2} \cdot \langle D_i^u, D_i^u \rangle \cdot \left(\frac{du}{dt}\right)^2$$

$$= D_i^u \cdot \langle D_i^u, D_i^u \rangle \cdot \frac{d^2u}{dt^2} + D_i^{u2} \cdot \langle D_i^t, D_i^t \rangle$$

or

$$D_i^{t2} = D_i^u \cdot \frac{d^2u}{dt^2} + D_i^{u2} \cdot \frac{\langle D_i^t, D_i^t \rangle}{\langle D_i^u, D_i^u \rangle} \tag{8}$$

where $<\,,\,>$ is an inner product operator. Since the curve parameter u is a time function, the approximation by using Taylor's expansion up to the second derivative is given by

$$u_{i+1} = u_i + \frac{du}{dt}\bigg|_{t=t_i} \cdot (t_{i+1} - t_i)$$

$$+ \frac{1}{2} \cdot \frac{d^2u}{dt^2}\bigg|_{t=t_i} \cdot (t_{i+1} - t_i)^2 + H.O.T \tag{9}$$

Substituting (5)–(8) into (9) and neglecting the higher order terms (*H.O.T.*) in (9), we can rewrite (9) as follows:

$$D_i^u \cdot u_{i+1}$$

$$= D_i^u \cdot u_i + D_i^u \cdot \frac{du}{dt}\bigg|_{t=t_i} \cdot (t_{i+1} - t_i) + \frac{1}{2} \cdot D_i^u \cdot \frac{d^2u}{dt^2}\bigg|_{t=t_i} \cdot (t_{i+1} - t_i)^2$$

$$= D_i^u \cdot u_i + D_i^t \cdot (t_{i+1} - t_i) + \frac{1}{2} \cdot D_i^u \cdot \frac{d^2u}{dt^2}\bigg|_{t=t_i} \cdot (t_{i+1} - t_i)^2 \tag{10}$$

Substituting (8) into (10), we can further rewrite (10) as follows:

$$D_i^u \cdot u_{i+1} = D_i^u \cdot u_i + D_i^t \cdot (t_{i+1} - t_i)$$

$$+ \frac{1}{2} \cdot \left(D_i^{t2} - D_i^{u2} \cdot \frac{\langle D_i^t, D_i^t \rangle}{\langle D_i^u, D_i^u \rangle}\right) \cdot (t_{i+1} - t_i)^2 \tag{11}$$

Let the time step in the interpolation be T_s seconds and

$$t_{i+1} - t_i = T_s$$

Then, the parameter iteration algorithm can be obtained from (11) by

$$u_{i+1} = u_i + \frac{\left\langle D_i^u, D_i^t \right\rangle}{\left\langle D_i^u, D_i^u \right\rangle} \cdot T_s$$

$$+ \frac{1}{2} \cdot \left(\frac{\left\langle D_i^u, D_i^{t2} \right\rangle}{\left\langle D_i^u, D_i^u \right\rangle} - \frac{\left\langle D_i^u, D_i^{u2} \right\rangle \cdot \left\langle D_i^t, D_i^t \right\rangle}{\left\langle D_i^u, D_i^u \right\rangle^2} \right) \cdot T_s^2 \qquad (12)$$

Because

$$\left\langle D_i^u, D_i^t \right\rangle = V(u_i) \cdot \left\| D_i^u \right\| ; \left\langle D_i^u, D_i^u \right\rangle = \left\| D_i^u \right\|^2$$

$$\left\langle D_i^u, D_i^{t2} \right\rangle = 0 ; \left\langle D_i^t, D_i^t \right\rangle = V^2(u_i)$$

Equation (12) can be rewritten as follows:

$$u_{i+1} = u_i + \frac{V(u_i) \cdot T_s}{\left\| D_i^u \right\|} - \frac{1}{2} \cdot \frac{\left\langle D_i^u, D_i^{u2} \right\rangle \cdot V^2(u_i) \cdot T_s^2}{\left\| D_i^u \right\|^4} \qquad (13)$$

where $V(u_i)$ is the curve speed along the tangent at $u = u_i$ and $\|\cdot\|$ is the Euclidean norm operator. Equation (13) can be further simplified to the first order by

$$u_{i+1} = u_i + \frac{V(u_i) \cdot T_s}{\left\| D_i^u \right\|} \qquad (14)$$

Equations (13) and (14) are the expressions of the parameter iteration method in this study. For the given u_i, T_s, and $V(u_i)$ and curve information such as D_i^u and D_i^{u2}, the parameter u_{i+1} can be obtained from (13) or (14).

For computing the motion commands such as the linear velocity $v(t)$ and the angular velocity $\dot{\theta}(t)$ at time $t = t_i$, the interpolated point $C(u_{i+1})$ must be calculated by using the iteration method shown in (13) or (14). Suppose that $C(u_{i-1})$, $C(u_i)$, and $C(u_{i+1})$ are the successive and adjacent interpolated points given as

$$C(u_{i-1}) = C(u)\big|_{u=u_{i-1}} ; u_{i-1} = u(t)\big|_{t=t_{i-1}}$$

$$C(u_i) = C(u)\big|_{u=u_i} ; u_i = u(t)\big|_{t=t_i}$$

$$C(u_{i+1}) = C(u)\big|_{u=u_{i+1}} ; u_{i+1} = u(t)\big|_{t=t_{i+1}}$$

Then, as shown in Fig. 6, the length α_i and the angle β_i are computed by

$$\alpha_i = \left\| C(u_{i+1}) - C(u_i) \right\|$$

$$\beta_i = \sin^{-1}\left(\frac{[C(u_i) - C(u_{i-1})] \times [C(u_{i+1}) - C(u_i)]}{\left\| C(u_i) - C(u_{i-1}) \right\| \cdot \left\| C(u_{i+1}) - C(u_i) \right\|} \right)$$

where $\times$ is a cross product operator. The linear velocity $v(t)$ and the angular velocity $\dot{\theta}(t)$ at time $t = t_i$ are obtained by

$$v(t_i) = v(t)\big|_{t=t_i} = \frac{\alpha_i}{T_s} \qquad (15)$$

$$\dot{\theta}(t_i) = \dot{\theta}(t)\big|_{t=t_i} = \frac{\beta_i}{T_s} \qquad (16)$$

where T_s is the time step in interpolation and is also the sampling period in control system. By using the iteration method shown in (13) or (14) with the given curve speed $V(u_i)$, the linear velocity $v(t_i)$ can be approximated to the given curve speed $V(u_i)$. For paths with large radii of curvature, the iteration method in (14) can provide good

approximation results. However, for paths with small radii of curvature, the iteration method in (13) should be considered for obtaining good approximation results. In this study, the given curve speed $V(u)$ at time $t = t_i$ is the desired linear velocity v_d defined in the motion control laws (described in section VI) such that the robotic cane can execute different motions according to the selected operation modes. Since the desired linear velocity v_d is a function of the interactive forces between the user and the robotic cane, the interpolation algorithm developed in this section can be used to generate motion commands that are closely related to the interactive forces. Thus, the force-controlled motion command generator developed by applying the interpolation algorithm can generate motion commands closely related to the interactive forces.

VI. DESIGN OF OPERATION MODES AND MOTION CONTROL LAWS

The robotic cane can provide two operation modes: AMM and MMM. These two operation modes are described as follows.

A. Autonomous Motion Mode (AMM)

The operation in the AMM can autonomously move the robotic cane through a preplanned motion path with a given velocity trajectory. Fig. 7 shows the operation setup of the robotic cane when it executes the AMM mode. As shown in Fig. 7, since a user's hand holds the handgrip of the cane-stick, the robotic cane can support and guide the user's walk depending on the motion of the mobile platform. For instance, the user walks forward when the mobile platform moves forward according to the preplanned motion paths. During the operation in the AMM mode, the selection of the motion path of the mobile platform depends on the status of the range sensors, as shown in Fig. 4 and Table I, and the robotic cane can thus guide users while avoiding collisions with obstacles.
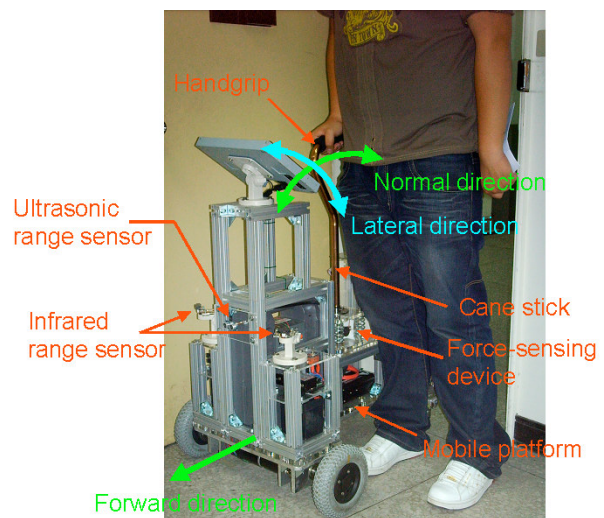

Fig. 7. Operation setup of the robotic cane.

Motion control laws of the robotic cane are designed by using the kinematics of the two-wheeled mobile platform. Fig. 8 illustrates the configuration of the two-wheeled mobile platform used in this study. In Fig. 8, P denotes the point centered between two drive-wheels, and L denotes the

distance of each wheel from the point *P*. *R* denotes the radius of wheels. ω_r and ω_l are the spinning speeds of right and left wheels, respectively. v and $\dot{\theta}$ represent the linear velocity and the angular velocity of point *P*, respectively. Therefore, for a given radius *R* and distance *L*, the relationship between velocities, v and $\dot{\theta}$, and spinning speeds, ω_r and ω_l, can be derived as

$$\begin{bmatrix} \omega_l \\ \omega_r \end{bmatrix} = \begin{bmatrix} \dfrac{1}{R} & -\dfrac{L}{2R} \\ \dfrac{1}{R} & \dfrac{L}{2R} \end{bmatrix} \begin{bmatrix} v \\ \dot{\theta} \end{bmatrix}. \tag{17}$$

Moreover, by using (17), the spinning speeds of all wheels can be obtained for the given values of velocities, v and $\dot{\theta}$, which are the motion commands generated by the motion command generator. For AMM mode operation, since the path and trajectory of the robotic cane are determined in advance according to the selected motion path and the desired linear velocity v_d, the desired spinning speeds, ω_r^d and ω_l^d, can be calculated by using (17) with the motion commands, v and $\dot{\theta}$, generated by the motion command generator, as shown in (15) and (16). The desired spinning speeds are speed commands for the drive wheels, as shown in Fig. 3.
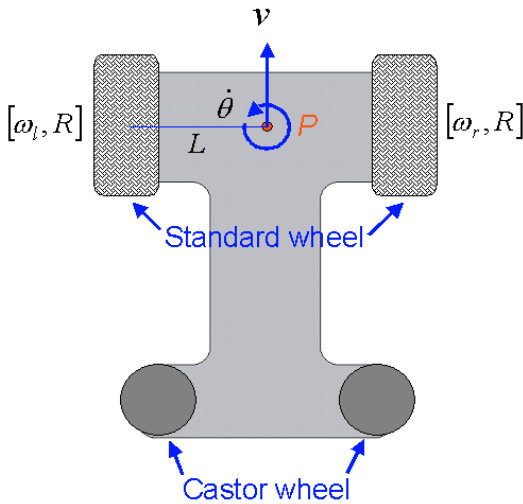

Fig. 8. Configuration of the applied mobile platform.

B. Manual Motion Mode (MMM)

The MMM makes it possible for the motion of the robotic cane to be driven by users. Thus, the users can walk at will with the assistance of the robotic cane. Fig. 7 also shows the operation setup of the robotic cane when it executes the MMM mode. The cane-stick and the mobile platform are connected through the biaxial force-sensing device. When the user operates the cane-stick by hand, the biaxial force-sensing device detects the direction and estimates the magnitude of the equivalent forces exerted by the user. The direction of the exerted forces is used to select the motion paths of the robotic cane, as shown in Fig. 5 and Table II. The magnitude of the equivalent forces is used to drive the mobile platform along the selected motion paths.

Equation (17) is also used to design the motion control law for MMM operation. However, in comparison with the AMM, only the motion path of the robotic cane is determined in

advance in the MMM; the desired linear velocity v_d is a function of the equivalent forces F_{app} as

$$v_d = f(F_{app}). \tag{18}$$

The desired spinning speeds that are the speed commands for the drive wheels can also be calculated by using (17) and the motion commands generated by motion command generator, as shown in (15) and (16).

The function $f(\cdot)$ in (18) significantly affects the motion performances of the robotic cane. The simplest function is a constant gain. For the function with a large constant gain, the user's hand can drive the robotic cane by exerting small forces on the force-sensing device. However, the motion of the robotic cane becomes sensitive to the motion of the user's hand, and the motion performances of the robotic cane are not good for some users such as Parkinson's patients. On the contrary, for the function with a small constant gain, the user's hand must drive the robotic cane by exerting large forces on the force-sensing device, and thus the motion of the robotic cane becomes less sensitive to the motion of the user's hand. Therefore, a low-pass filter with adjustable gain and adjustable bandwidth is suitable for most applications. The low-pass filter can reduce perturbations exerted by the user's hand, and it can also adjust the motion sensitivity of the robotic cane. By setting suitable gain and bandwidth of the applied low-pass filter function, the robotic cane operated in the MMM can provide smooth motion with good flexibility and safety for users walking in living environments.

VII. SIMULATION AND EXPERIMENTAL RESULTS

A. Simulations of Motion Command Generator

Fig. 9 shows the motion path for testing the motion command generator. The robotic cane moves along the forward direction path from the start point to the end point. Fig. 10 shows the computed linear velocity and angular velocity motion commands when the robotic cane moves along the motion path shown in Fig. 9. The desired linear velocity v_d (which is also the curve speed $V(u_i)$ during interpolation) is 6.5 cm/s in the beginning and it changes to 13.0 cm/s after few seconds. However, in real applications, the desired linear velocity will change according to the selected operation mode and the forces exerted by the user's hand. Clearly, the computed linear velocity is considerably similar to the desired linear velocity because the test motion path has a large radius of curvature. Usually, the motion paths of the robotic cane have a large radius of curvature for providing smooth motion of users' walking. The computed angular velocity is about 0.2 rad/s, and it changes to about 0.4 rad/s when the desired linear velocity is changed to 13.0 cm/s. The simulation results indicate that the motion command generator can generate linear velocity and angular velocity motion commands according to the selected motion path and the applied desired linear velocity v_d for controlling the robotic cane.
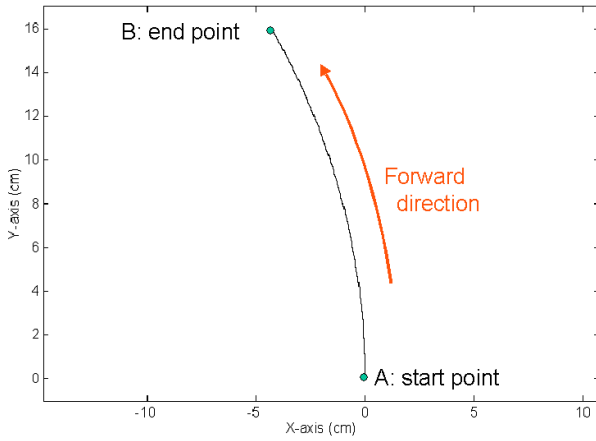
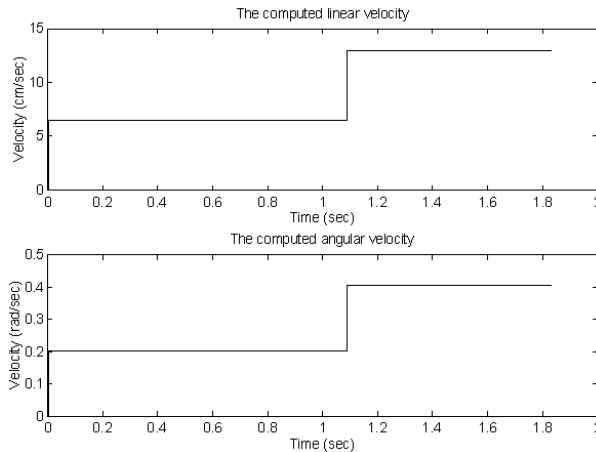Fig. 9. The test motion path of the robotic cane.

Fig. 10. The computed linear velocity and angular velocity motion commands.

B. Experimental Tests for Characterizing Biaxial Force-sensing Device

Fig. 11 illustrates the experimental setup for characterizing the biaxial force-sensing device. In order to characterize the spring coefficient of the force-sensing device on different directions, several test points such as test point A to test point H are marked on the upper plate of the device. The test points are all at equal distance d from the central point of the upper plate. In the tests, the distance d is 5.0 cm and the test points are distributed as shown in Fig. 11.
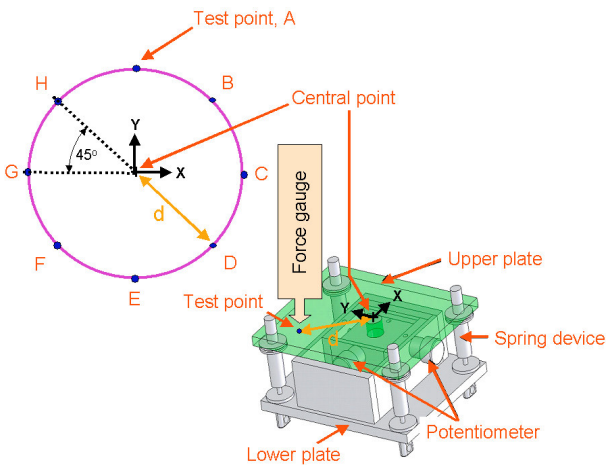
Fig. 11. The experimental setup for characterizing the biaxial force-sensing device.

A force gauge LUTRON FG-5020 is used to apply test forces to the test points and to measure the magnitude of the applied forces. The applied force gauge has the following specifications:

- Maximum measuring push/pull force is 220 N
- Force measuring resolution is 0.05 N
- Force measuring accuracy is 0.5%

Two potentiometers are used to detect the relative angular movements between the upper and lower plates when the test forces are applied to the test points through the force gauge. By measuring the detected voltages of two potentiometers, the magnitude of the measured voltage V_{mag} is obtained as

$$V_{mag} = \sqrt{V_x^2 + V_y^2} \tag{19}$$

where V_x and V_y are the detected relative voltages corresponding to the relative angular movements along the X and Y directions, respectively.

The virtual spring coefficient K_{spring} in this study is defined as the ratio of the applied test force F_{test} to the magnitude of the measured voltage V_{mag}^{test}. The voltage V_{mag}^{test} is obtained from (19) with the detected voltages of two potentiometers when the test force F_{test} is applied to the test point. The virtual spring coefficient K_{spring} is varied depending on the location of the test point. Moreover, because the manufacture and the assembly of the force-sensing device are usually not good enough, the detected relative voltages, V_x and V_y, are not orthogonal. Thus, the angle between the detected voltages, V_x and V_y, is used as the reference parameter in real applications. The detected angle ϕ is obtained by

$$\phi = \tan^{-1}\left(\frac{V_y}{V_x}\right) \tag{20}$$

and thus the virtual spring coefficient K_{spring} becomes the function of the detected angle ϕ. Thus, $K_{spring} = K_{spring}(\phi)$.

In order to obtain the function of the virtual spring coefficient, $K_{spring}(\phi)$, the test force F_{test} is applied to different test points, and the corresponding magnitude V_{mag}^{test} and angles ϕ are recorded as shown in Table III. Since the relative angular movements between the upper and lower plates are usually small, the detected voltages of the two potentiometers must be amplified in actual applications. The function of the virtual spring coefficient $K_{spring}(\phi)$ is obtained by using the least-squares curve fitting method to fit the data in the fourth and the fifth columns of Table III. Equation (21) shows the fitted coefficient function and Fig. 12 illustrates the function.

$$\begin{aligned} K_{spring}(\phi) = &-1.8215\times10^{-9}\phi^7 + 2.3443\times10^{-6}\phi^6 \\ &-1.2771\times10^{-3}\phi^5 + 3.8178\times10^{-1}\phi^4 \\ &-6.7633\times10^{1}\phi^3 + 7.1012\times10^{3}\phi^2 \\ &-4.0922\times10^{5}\phi^1 + 9.9870\times10^{6} \end{aligned} \tag{21}$$

Since Fig. 12 shows the region with negative spring coefficient and the region with large spring coefficient, the function of the virtual spring coefficient $K_{spring}(\phi)$ is

modified as shown in (22) for providing safe motions of the robotic cane.

$$\hat{K}_{spring}(\phi) = -1.8215 \times 10^{-9} \phi^7 + 2.3443 \times 10^{-6} \phi^6$$
$$- 1.2771 \times 10^{-3} \phi^5 + 3.8178 \times 10^{-1} \phi^4$$
$$- 6.7633 \times 10^1 \phi^3 + 7.1012 \times 10^3 \phi^2 \qquad (22)$$
$$- 4.0922 \times 10^5 \phi^1 + 9.9870 \times 10^6$$

$$K_{spring}(\phi) = \begin{cases} K_{spring}^{upper}, & \hat{K}_{spring}(\phi) \geq K_{spring}^{upper} \\ 0, & \hat{K}_{spring}(\phi) < 0 \\ \hat{K}_{spring}(\phi), & \text{otherwise} \end{cases}$$

In (22), the upper limit K_{spring}^{upper} is designed by experiments, and it is 600.0 N/Volt in this study.

Since relative angular movements between the upper and lower plates occur when the user's hand exerts forces on the force-sensing device, the magnitude of the measured voltage V_{mag} can be obtained by (19), and the detected angle ϕ can be obtained by (20). The virtual spring coefficient $K_{spring}(\phi)$ can be obtained by (22). In this study, the equivalent force F_{app} used to control the mobile platform of the robotic cane is obtained as

$$F_{app} = K_{spring}(\phi) \cdot V_{mag} \qquad (23)$$

Moreover, in this study, the detected angle ϕ shown in (20) is used to select the motion path of the robotic cane, as shown in Fig. 5 and Table II. If the detect angle generated due to the operation of user's hand is near the detect angle of a test point, as shown in Table III, the sub-range corresponding to the test point, as shown in Fig. 5, is used to select the motion path according to Table II. For instance, if the detect angle generated due to the operation of user's hand is near the detected angle of test point A, the sub-range "R3" is used to select the motion path "Path F" for the robotic cane.
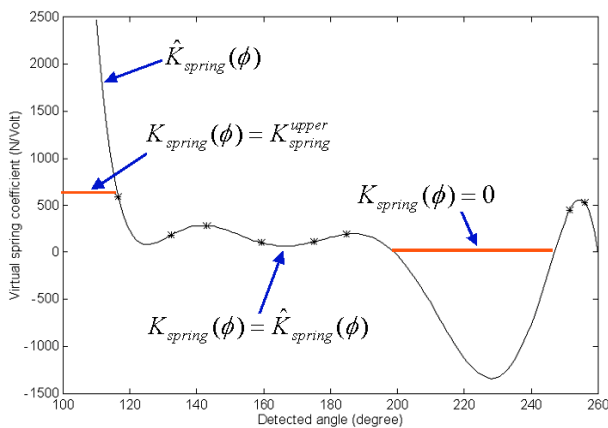

Fig. 12. The function of the virtual spring coefficient.

TABLE III
EXPERIMENTAL RESULTS OF THE BIAXIAL FORCE-SENSING DEVICE

Test point	Test force F_{test} (N)	Detected magnitude V_{mag}^{test} (Volt)	Detected angle ϕ (Degree)	Virtual spring coefficient K_{spring} (N/Volt)
A	210.65	1.13	132.51	184.85
B	184.55	0.31	116.56	589.52
C	196.05	0.70	143.13	280.00
D	152.50	0.28	255.96	528.38
E	197.45	0.44	251.56	445.99
F	160.55	0.84	184.76	190.47
G	190.15	1.68	175.23	112.79
H	180.20	1.79	159.44	100.43

C. Autonomous Motion Mode (AMM) Tests

Figs. 13–17 show the experimental results when the robotic cane executes the AMM mode. The desired linear velocity is 10.0 cm/s. As shown in Figs. 13 and 14, although the force-sensing device equipped on the robotic cane detects the forces exerted by the user's hand, the robotic cane still executes the desired motion according to the desired linear velocity. However, as shown in Figs. 15–17, the motion of the robotic cane changes according to the status of the applied infrared range sensors. The robotic cane turns to the left with a positive angular velocity, as shown in Fig. 16, when the right infrared range sensor detects obstacles on the front-right side of the robotic cane, as shown in Fig. 17; the robotic cane turns to the right with negative angular velocity when the left infrared range sensor detects obstacles on the front-left side of the robotic cane. The linear velocity response exhibits fluctuation, as shown in Fig. 15, because the selected motion paths of the robotic cane periodically change according to the status of the applied range sensors.
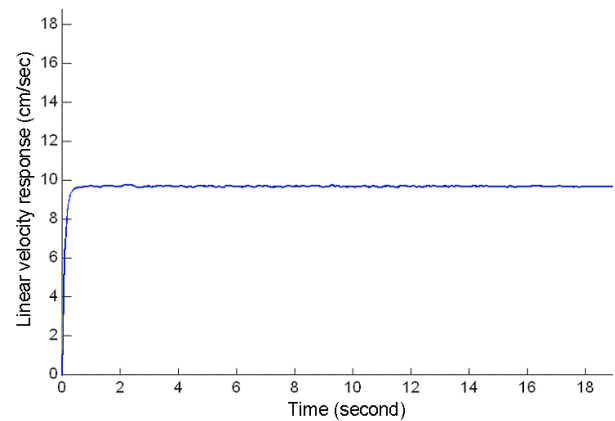

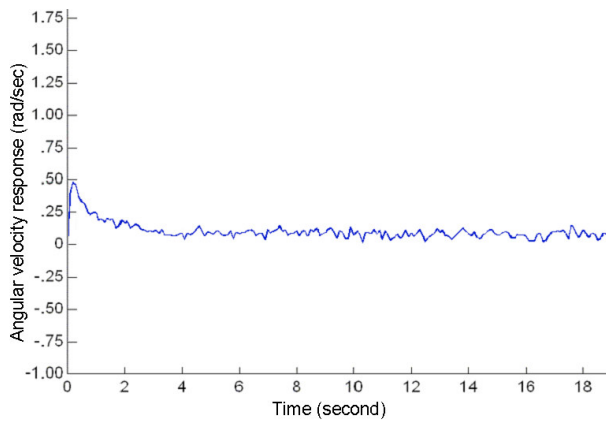Fig. 13. Linear velocity response of the robotic cane (AMM mode).

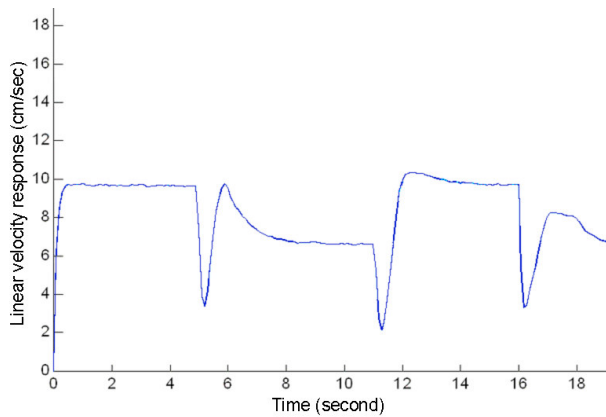Fig. 14. Angular velocity response of the robotic cane (AMM mode).

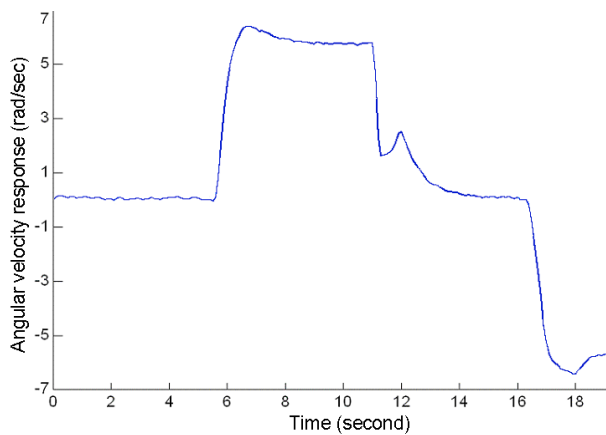Fig. 15. Linear velocity response of the robotic cane with obstacles (AMM mode).

Fig. 16. Angular velocity response of the robotic cane with obstacles (AMM mode).
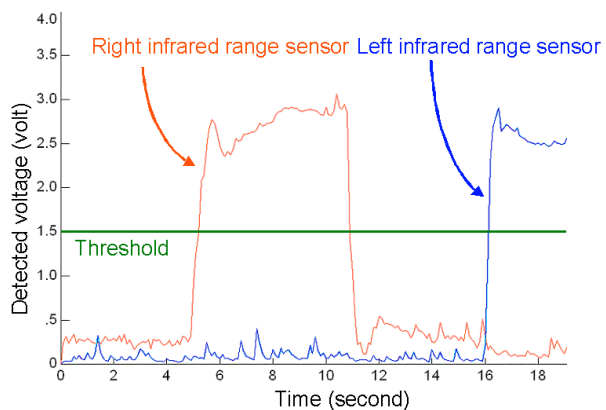

Fig. 17. Detection of the applied infrared range sensors (AMM mode).

D. Manual Motion Mode (MMM) Tests

Figs. 18–24 show the experimental results when the robotic cane executes the MMM mode. During the operation in the MMM mode, the forces exerted by the user's hand drive the robotic cane, as shown in Figs. 18–20. The linear velocity response of the robotic cane, as shown in Fig. 18, thus has signal patterns similar to those of the magnitude of the measured voltages using the biaxial force-sensing device, as shown in Fig. 20. Fig. 19 shows that the angular velocity response of the robotic cane fluctuates around zero because the selected motion path is straightforward.
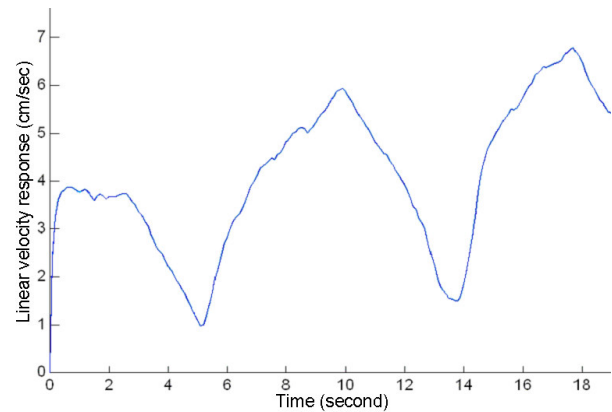

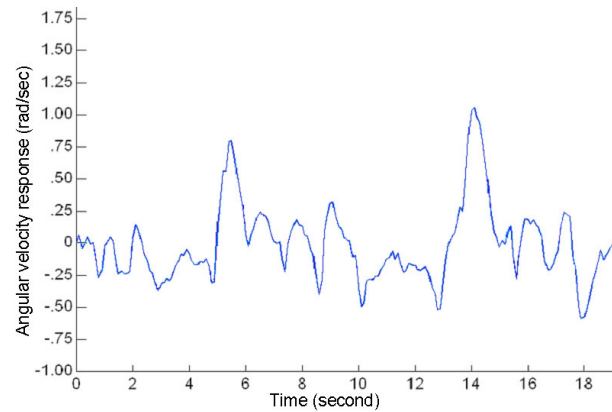Fig. 18. Linear velocity response of the robotic cane (MMM mode).

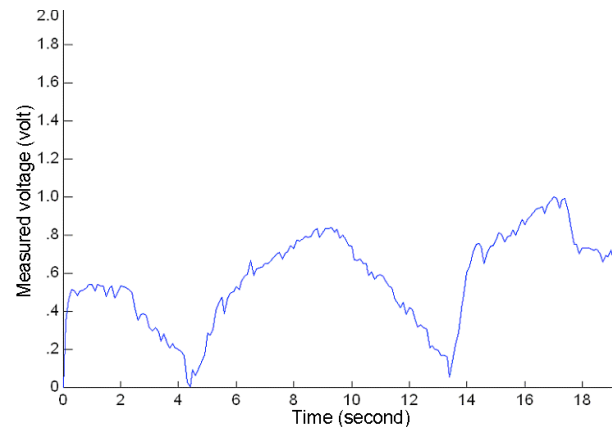Fig. 19. Angular velocity response of the robotic cane (MMM mode).

Fig. 20. Magnitude of the measured voltage (MMM mode).

Although the forces exerted by the user's hand can drive the robotic cane during the operation in the MMM mode, the status of the applied range sensors affects the motion of the robotic cane when obstacles appear in front of the robotic cane. As shown in Figs. 21–24, since there are no obstacles located in front of the robotic cane at the beginning 8 s, the

user's hand drives the robotic cane through the biaxial force-sensing device, and thus the linear velocity response of the robotic cane, as shown in Fig. 21, has signal patterns similar to those of the magnitude of the measured voltages, as shown in Fig. 24. However, after 8 s, although the biaxial force-sensing device detects the equivalent forces exerted by the user's hand, as shown in Fig. 24, the motion of the robotic cane changes according to the status of the infrared ranger sensors. The robotic cane turns to the left, as shown in Fig. 22, when the right infrared range sensor detects obstacles, as shown in Fig. 23, and the robotic cane turns to the right when the left infrared range sensor detects obstacles. The fluctuation of the linear velocity response is due to the periodically changing motion paths.
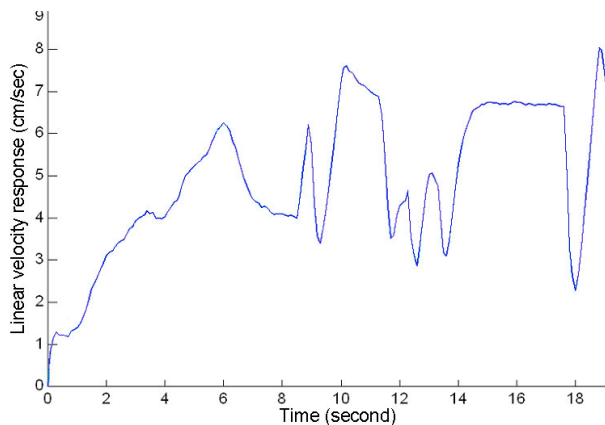

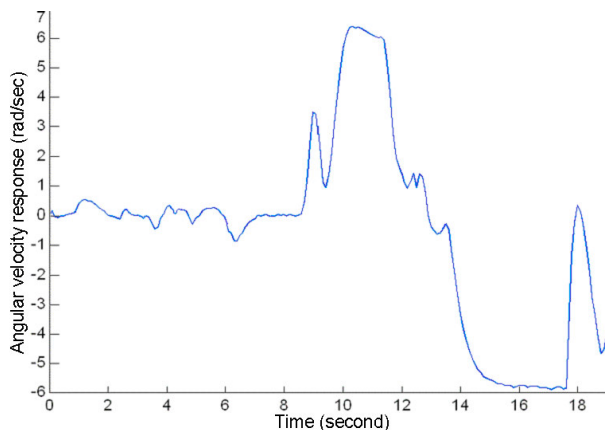Fig. 21. Linear velocity response of the robotic cane with obstacles (MMM mode).

Fig. 22. Angular velocity response of the robotic cane with obstacles (MMM mode).
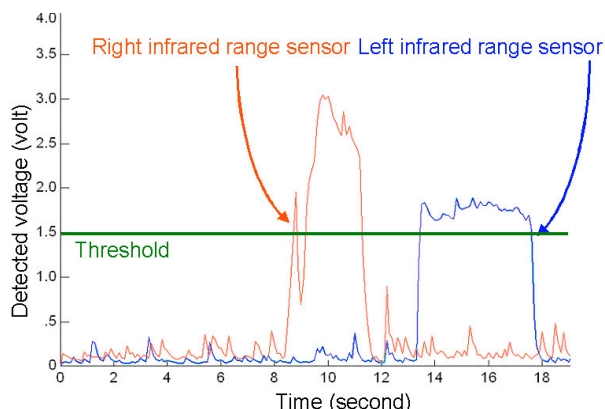

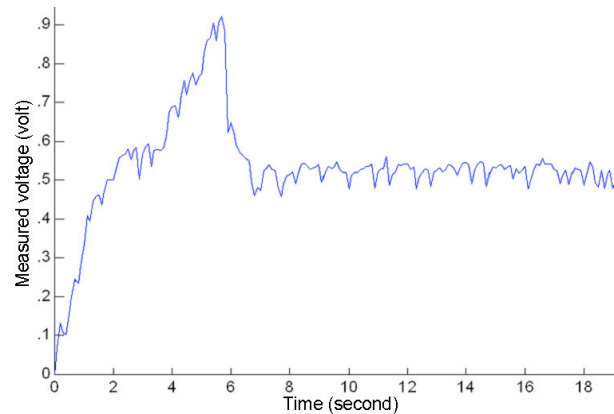Fig. 23. Detection of the applied infrared range sensors (MMM mode).

Fig. 24. Magnitude of the measured voltage (MMM mode).

VIII. CONCLUSION

Even though some high-level functions have been successfully developed to augment the auxiliary capabilities of robotic walking support systems, motion control design continues to be essential and important because it directly affects the steps users take during motion. In this study, a force-controlled motion command generator is developed for the motion control design of robotic walking support systems. Through the cooperation of motion control laws and force-sensing results by the force-controlled motion command generator, the robotic walking support system can move smoothly at the desired motion speed. It can thus physically support and smoothly guide users, especially the elderly, in general applications. A low-pass filter with adjustable gain and adjustable bandwidth is applied to the design of motion control laws. Moreover, for estimating the applied forces exerted by the user's hand, a simple and low-cost biaxial force-sensing device is developed in this study. For a given virtual spring coefficient obtained from the calibration procedure, the magnitude and direction of the equivalent applied forces are estimated and applied to control the robotic walking support system through the force-controlled motion command generator.

In order to test the proposed motion control approach, a robotic walking support system, a robotic cane, is developed in this study with the following two modes of operation:

- Autonomous motion mode (AMM): the robotic cane autonomously moves in living environments according to the preplanned motion paths and the status of the applied range sensors.
- Manual motion mode (MMM): the user can manipulate the robotic cane through the biaxial force-sensing device and motion control laws such that the motion of the robotic cane depends on the user's decision.

Some simulations and experimental tests are conducted on the robotic cane to evaluate the execution performances of the proposed motion control approach. The experimental results indicate that the robotic cane can execute design functions according to the selected operation modes. These results thus show the validity of the proposed motion control approach.

REFERENCES

[1] G. Lacey and K. M. Dawson-Howe, "The Application of robotics to a mobility aid for the elderly blind," *Robotics and Autonomous Systems,* vol. 23, no. 4, pp. 245–252, 1998.

[2]   S. MacNamara and G. Lacey, "A Smart walker for the frail visually impaired," *Proc. of the 2000 IEEE International Conference on Robotics and Automation,* vol. 2, pp. 1354–1359, 2000.

[3]   B. Graf, M. Hans, and R. D. Schraft, "Care-O-bot II - Development of a Next Generation Robotic Home Assistant," *Autonomous Robots,* vol. 16, no. 2, pp. 193–205, 2004.

[4]   Y. Hirata, A. Hara, and K. Kosuge, "Motion control of passive intelligent walker using servo brakes," *IEEE Transactions on Robotics,* vol. 23, no. 5, pp. 981–990, 2007.

[5]   O. Chuy Jr., Y. Hirata, and K. Kosuge, "Online approach in adapting user characteristic for robotic walker control," *Proc. of the 2005 IEEE 9th International Conference on Rehabilitation Robotics,* vol. 2005, pp. 139–142, 2005.

[6]   O. Chuy Jr., Y. Hirata, and K. Kosuge, "A new control approach for a robotic walking support system in adapting user characteristics," *IEEE Transactions on Systems, Man and Cybernetics Part C: Applications and Reviews,* vol. 36, no. 6, pp. 725–733, 2006.

[7]   O. Chuy Jr., Y. Hirata, Z. Wang, and K. Kosuge, "A control approach based on passive behavior to enhance user interaction," *IEEE Transactions on Robotics,* vol. 23, no. 5, pp. 899–908, 2007.

[8]   G. Wasson, P. Sheth, M. Alwan, K. Granata, A. Ledoux, and C. Huang, "User Intent in a Shared Control Framework for Pedestrian Mobility Aids," *Proc. of the 2003 IEEE International Conference on Intelligent Robots and Systems,* vol. 3, pp. 2962–2967, 2003.

[9]   A. Morris, R. Donamukkala, A. Kapuria, A. Steinfeld, J. T. Matthews, J. Dunbar-Jacob, and S. Thrun, "A robotic walker that provides guidance," *Proc. of the 2003 IEEE International Conference on Robotics and Automation,* vol. 1, pp. 25–30, 2003.

[10] A. M. Sabatini, V. Genovese, and E. Pacchierotti, "A mobility aid for the support to walking and object transportation of people with motor impairments," *Proc. of the 2002 IEEE International Conference on Intelligent Robots and Systems,* vol. 2, pp. 1349–1354, 2002.

[11] M. Spenko, H. Yu, S. Dubowsky, "Robotic personal aids for mobility and monitoring for the elderly," *IEEE Transactions on Neural Systems and Rehabilitation Engineering,* vol. 14, no. 3, pp. 344–351, 2006.

[12] M.-J. Yoon, K.-H. Yu, J.-H. Kang, and N.-G. Kim, "Walking guide robot with tactile display for the blind," *Proc. of the SPIE - The International Society for Optical Engineering,* vol. 6040, ICMIT 2005: Mechatronics, MEMS and Smart Materials, pp. 60402A, 2005.

[13] I. Shim, J. Yoon, and M. Yoh, "A human robot interactive system 'RoJi'," *International Journal of Control, Automation and Systems,* vol. 2, no. 3, pp. 398–405, 2004.

[14] S. Shoval, I. Ulrich, and J. Borenstein, "Robotics-Based Obstacle-Avoidance Systems for the Blind and Visually Impaired: NavBelt and the GuideCane," *IEEE Robotics and Automation Magazine,* vol. 10, no. 1, pp. 9–20, 2003.

[15] P. Aigner and B. McCarragher, "Shared control framework applied to a robotic aid for the blind," *Proc. of the 1998 IEEE International Conference on Robotics and Automation,* vol. 1, pp. 717–722, 1998.

[16] Y. Z. Zhang and S. S. Yeh, "Motion Control Design for Robotic Walking Support Systems Using Admittance Motion Command Generator," *Lecture Notes in Engineering and Computer Science: Proc. of The International MultiConference of Engineers and Computer Scientists 2011*, vol. 2, pp. 781-786, 2011.